Struct Bond (2014) 161: 87–116
DOI: 10.1007/430_2014_146

Published online: 15 April 2014

Gold Nanoclusters: Size-Controlled Synthesis and Crystal Structures

Chenjie Zeng and Rongchao Jin

Abstract One of the major goals in nanoparticle research is to investigate their unique properties not seen in bulk materials or small molecules. In this chapter, we focus on a new class of gold nanoparticles (often called nanoclusters) that possess atomic precision (as opposed to conventional nanoparticles with a size distribution). The synthetic methods for obtaining atomically precise thiolate-protected gold nanocluters are first discussed, followed by the anatomy of the X-ray crystal structures of gold nanoclusters.

Keywords Atomic precision · Crystal structure · Gold · Nanocluster · Size-focusing · Thiol

Contents

C. Zeng and R. Jin (✉)
Department of Chemistry, Carnegie Mellon University, 4400 Fifth Ave, Pittsburgh, PA 15213, USA
e-mail: rongchao@andrew.cmu.edu

1 Introduction

One of the major goals in nanoparticle research is to investigate their unique properties not seen in bulk materials or small molecules. By tailoring the size or shape of nanoparticles, their physical and chemical properties exhibit significant changes compared to bulk materials [1]. In terms of size control, there have been major advances in the last decade, and a wide range of monodisperse nanoparticles (e.g., 3–100 nm diameter) are now accessible.

Monodispersity is the most important criterion in terms of the quality of nanoparticles and is typically assessed by transmission electron microscopy (TEM) (Fig. 1a, b). The ultimate control over nanoparticles is to obtain atomically precise particles [2]. While such atomic monodispersity has not been realized for regular sized nanoparticles (e.g., >3 nm diameter), ultrasmall nanoparticles (1–3 nm, equivalent to a few tens to hundreds of atoms) are now possible to achieve atomic precision, for example, 25-gold-atom nanoparticles (1 nm metal core diameter (Fig. 1c). The atomic monodispersity of nanoparticles is assessed by mass spectrometry (Fig. 1d). These ultrasmall nanoparticles are often called nanoclusters to distinguish from regular nanoparticles.

The term "monodispersity" used in nanochemistry is not as precise as the term "purity" in molecular chemistry. A pure compound should be free of impurities and also with a definite chemical formula. For molecularly pure nanoclusters, all the particles should have the same molecular weight and the same formula, i.e. "atomic precision." It has long been a major dream for nanochemists to prepare atomically precise nanoparticles. Such nanoparticles will be absolutely monodisperse and uniform at the atomic scale and thus can be treated as giant molecules. When all the nanoparticles in a sample are atomically monodisperse, mass spectrometry analysis will show a single molecular weight (Fig. 1d). Hence, the atomic precision is a stricter and more accurate criterion than the conventional term "monodispersity" used for regular nanoparticles, and correspondingly, mass spectrometry is a more accurate characterization tool than TEM and is indeed indispensible in nanocluster characterization.

To make atomically precise nanoclusters is of paramount importance for understanding the fundamental science of nanoclusters [3]. For molecularly pure nanoclusters, many well-established characterization tools in the traditional molecular chemistry can be applied and provide in-depth characterization. For example, one can employ mass spectrometry (e.g., electrospray ionization mass spectrometry, ESI-MS, and matrix-assisted laser desorption ionization mass spectrometry, MALDI-MS) to unambiguously determine the molecular weight of nanoclusters [3–6], single-crystal X-ray crystallography to determine the total structure of nanoclusters [7–13], nuclear magnetic resonance (NMR) spectroscopy to probe organic ligand environment and metal core chirality [14, 15], and so forth. These molecular characterization tools lead to fundamental understanding of the physical and chemical properties of atomically precise nanoclusters.

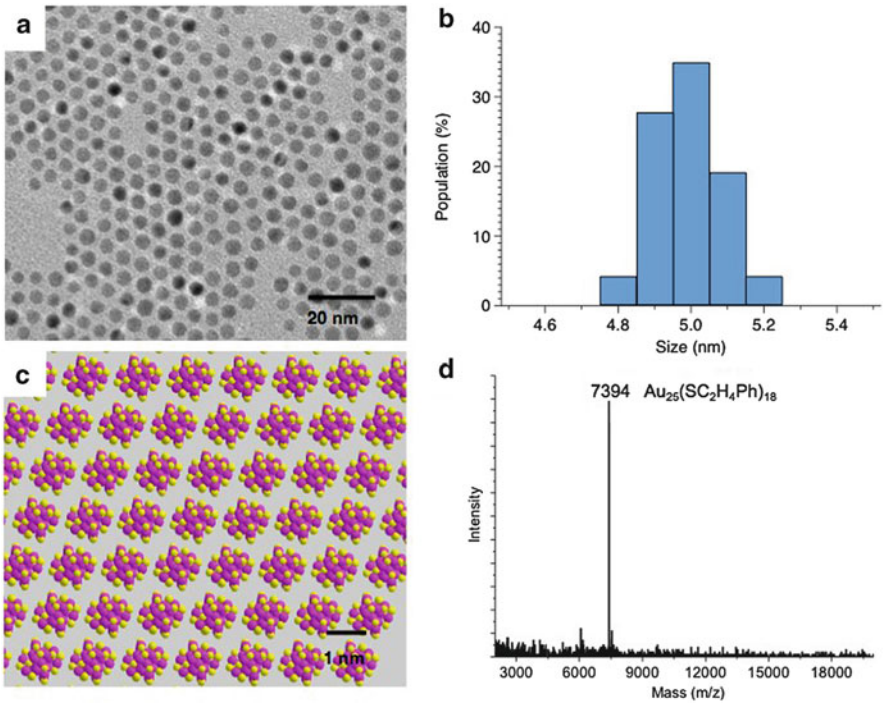

Fig. 1 (**a**) Monodisperse nanoparticles imaged by TEM; (**b**) histogram of size distribution (5 ± 0.3 nm diameter); (**c**) atomically precise $Au_{25}(SC_2H_4Ph)_{18}$ nanoclusters (1 nm metal core diameter, $-C_2H_4Ph$ groups are omitted, magenta = Au, yellow = S); (**d**) mass spectrometry characterization of $Au_{25}(SC_2H_4Ph)_{18}$ nanoclusters

2 Ligand-Protected Gold Nanoclusters

In solution phase, nanoclusters must be protected by ligands or stabilizers; otherwise, unprotected nanoclusters would immediately aggregate, forming a precipitate and losing the integrity of individual nanoclusters. For nanochemists, a major task is to find appropriate ligands for stabilizing nanoclusters and more importantly enabling controlled synthesis.

The early research on gold nanoclusters involved phosphine as ligand. The gold-phosphine chemistry was developed as a derivative of the coordination chemistry, which started in the 1960s. As a spin-off of the research of gold:phosphine complex compounds, an eleven-gold-atom cluster, $Au_{11}(PPh_3)_7(SCN)_3$, was reported in 1969 [16]. The Au_{11} structure exhibits an incomplete icosahedral framework. Mingos and coworkers predicted 13-atom-centered icosahedral cluster and successfully synthesized $[Au_{13}(PR_3)_{10}Cl_2]^{3+}$ and determined the structure in 1981 [17]. Schmid et al. reported $Au_{55}(PR_3)_{12}Cl_6$, although the structure has not been attained to date [18]. Teo et al. reported $[Au_{39}(PR_3)_{14}Cl_6]^{2+}$ and bimetal nanoclusters such as $[Au_{13}Ag_{12}(PR_3)_{10}Br_8]^{+}$, $[Au_{18}Ag_{19}(PR_3)_{12}Br_{11}]^{2+}$, and

$[Au_{18}Ag_{20}(PR_3)_{14}Cl_{12}]^{2+}$ [19–22]. Dahl and coworkers synthesized and characterized a series of phosphine-carbonyl Pd_n nanoclusters [23–26].

In recent development of gold-phosphine nanoclusters, Shichibu et al. reported diphosphine-protected Au_{13} icosahedral clusters [27]. Pettibone et al. carried out detailed work on the synthesis and growth mechanism of small gold-phosphine clusters [28]. Wan et al. reported the structure of $[Au_{20}(PPhpy_2)_{10}Cl_4]^{2+}$ cluster (where $Phpy_2$ = pyridyl phosphine), in which the core consists of two edge-shared Au_{11} units [29]. With phosphine/thiolate ligands, a biicosahedral $[Au_{25}(PPh_3)_{10}(SR)_5Cl_2]^{2+}$ cluster (SR = thiolate) has been obtained [30, 31]. Recently, Das et al. report a $[Au_{24}(PPh_3)_{10}(SC_2H_4Ph)_5X_2]^{+}$ nanocluster (where X = Cl/Br) [32]. Zheng and coworkers recently reported $Au_{13}Cu_x$ (x = 2, 4, 8) nanoclusters protected by mixed phosphine and thiolate ligands [33].

Thiol was extensively used in the synthesis of gold(I)-thiolate complexes in early research, and later thiol was used to prepare gold nanoparticles. In this chapter, we focus on the thiolate-protected *nanoclusters*, while the research on conventional gold-thiolate *nanoparticles* is not discussed herein.

3 Thiolate-Protected Gold Nanoclusters

The protecting molecules are very important for the stability of nanoclusters. Generally speaking, the protecting molecules provide barriers such as electrostatic and steric repulsions between particles to prevent them from aggregation into precipitate. Different types of protecting molecules impart different stability to nanoclusters. For conventional gold nanoparticles, simple ions (e.g., citrate), polymers, surfactants, as well as ligands have been used for stabilization (Fig. 2). Among these reagents, ligands – especially thiolate – render highly stable gold nanoparticles and nanoclusters, and thus are of wide interest. The high stability of thiolate-protected gold nanoparticles originates from the strong covalent bonding between thiolate and gold – the ligand is thus hard to dissociate from the nanoparticle surface. The carbon tails of the thiolate ligands provide further steric repulsion between nanoparticles, hence preventing aggregation.

The study of thiolate-protected gold nanoclusters experienced several stages, i.e. from polydispersed nanoclusters to monodispersed ones and finally to atomically precise nanoclusters [2, 34–37]. In early years, separation was done on the polydisperse nanoclusters in order to obtain relatively monodisperse ones [4, 35]. In recent years, the research progress has evolved to large-scale, controlled synthesis [37–43].

Whetten's group found that the thiolate-protected gold nanoclusters had the trend to form a series of *discrete* sizes [35]. The mixture of clusters was separated by solvent fractionation, and each fraction was characterized by laser desorption ionization mass spectrometry (LDI-MS). Distinct species with molecular weight of $5k$, $8k$, $14k$, $22k$, $29k$, etc., where k = 1,000 Da were identified; of note, these mass values correspond to the mass of Au_xS_y [36, 44–47]. Those species were quite

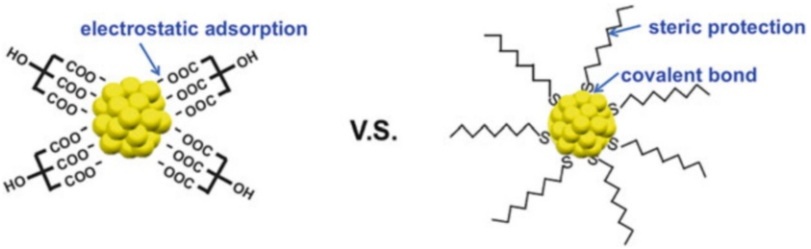

Fig. 2 Stability of traditional gold colloids (e.g., citrate-protected) and of thiolate-protected gold nanoparticles

monodispersed, but not atomically precise. No exact formula was assigned to those species due to fragmentation resulted by LDI-MS. For formula assignment, *intact* molecular ions (and hence accurate molecular weight) must be obtained first. Nevertheless, those early works on discrete gold nanocluster species provide valuable information and stimulation for later work for atomically precise nanoclusters.

With the improvement in the characterization techniques, especially the mass spectrometry, the accurate formula weights of gold nanoclusters were later obtained [4–6]. Combined with the improvement in the separation techniques, a series of "magic sizes" with well-defined chemical compositions were achieved, such as $Au_{25}(SR)_{18}$ and $Au_{38}(SR)_{24}$ (here SR represents thiolates generally) [4, 5, 48]. There are many other atomically precise species that were later obtained from separation [49–54]. However, it remained to devise synthetic methods for large-scale, controlled synthesis.

In recent years, great progress has been made in controlled synthesis of gold nanoclusters [37–43]. A systematic "size-focusing" methodology has been developed for attaining atomically precise nanoclusters with size control, based on earlier works that under harsh chemical and/or thermal conditions the initially polydispersed clusters could be size narrowed [37, 48, 55]. This methodology has led to direct syntheses of a series of atomically precise gold nanoclusters, including $Au_{25}(SR)_{18}$, $Au_{38}(SR)_{24}$, $Au_{144}(SR)_{60}$ and the largest ever $Au_{333}(SR)_{79}$ [38–41]. The development of the synthetic strategy greatly advanced the fundamental research on the optical and electronic properties of gold nanoclusters [9] as well as the applications of nanoclusters [56–59]. Below we shall give a detailed discussion on the size-focusing methodology for synthesizing atomically precise gold nanoclusters.

4 Size-Controlled Synthesis of Gold Nanoclusters with Atomic Precision

The chemistry for synthesizing gold-thiolate nanoclusters involves the reduction of a gold salt precursor by a reducing agent in the presence of thiol. The balance between growth and surface passivation controls the size of nanoclusters. Three chemicals are typically required in the synthesis of gold nanoclusters: the gold

precursor (e.g., $HAuCl_4$), protecting thiol ligand (e.g., HSR), and reducing agent (e.g., $NaBH_4$). However, to obtain atomically precise gold nanoclusters of molecular purity [3, 14, 15] is by no means easy. In nanochemistry, controlling the precise size and shape of nanoclusters is very difficult, for that during the reaction many factors can affect the size distribution of gold nanoclusters. For the static factors, examples are the concentration of gold precursor, the type of solvent used as reaction medium, the type and concentration of thiol, and the type and concentration of reducing agent, etc. For the dynamic factors, there are the reaction temperature, the stirring speed, the mixing of gold salt and ligand, the addition speed of the reductant, the reducing and aging time, etc. Tuning each of the above factors may result in different nanocluster products. Overall, for the synthesis of gold nanoclusters, the chemistry (i.e., reactions, mainly reduction of gold salt) is relatively simple, while the control over the subsequent growth of Au(0) atoms into well-defined nanoclusters can be quite complicated and requires significant efforts.

4.1 Size-Focusing Methodology

Among the synthetic methods for atomically precise gold nanoclusters, the recently established size-focusing methodology has been demonstrated to be quite universal [37]. There are two primary steps for a 'size-focusing' synthesis (Fig. 3). In step 1, polydispersed gold nanoclusters with a controlled size range are obtained through tuning the reaction conditions (i.e., the static and dynamic factors). In step 2, these initially polydispersed gold nanoclusters are focused into single-size product by aging/etching under a harsh environment.

The foundation of "size focusing" is based on the inherent stability difference of different-sized nanoclusters. Those stable sizes are sometimes called "magic sizes." When a harsh environment is applied to the mixture of nanoclusters, only the most robust species can survive size focusing, while the other species are either decomposed or converted to the most stable size [60]. The *'survival of the most robust'* principle somewhat resembles nature's law '*survival of the fittest*' [37].

With respect to the stability of magic-size nanoclusters, there are generally arguments invoking the geometric and electronic factors. For the geometric factor, certain geometric core arrangements (e.g., icosahedron) as well as the arrangement of surface thiolate ligands impart particular stability to the overall nanocluster structure. While for the electronic factor, those gold nanoclusters with the number of Au 6s free electrons satisfying electron-shell closing (i.e., $1S^21P^61D^{10}2S^2\ldots$) are regarded to be stable. This electron-shell picture resembles the electronic structure of atoms (i.e., $1s^22s^2p^6\ldots$). Some gold nanoclusters may be viewed as superatoms, such as anionic $[Au_{25}(SR)_{18}]^-$ [61], in which the number of Au 6s free electrons is counted as follows: 25 (the number of gold atoms) − 18 (the number of thiolate, each consumes 1e) + 1 (the anionic charge state) = 8e (consistent with $1S^21P^6$). But many exceptions exist, such as $[Au_{38}(SR)_{24}]^0$ (formal electron count: 14e, deviated from the closest 18e for $1S^21P^61D^{10}$). More discussions are in the Sect. 6.

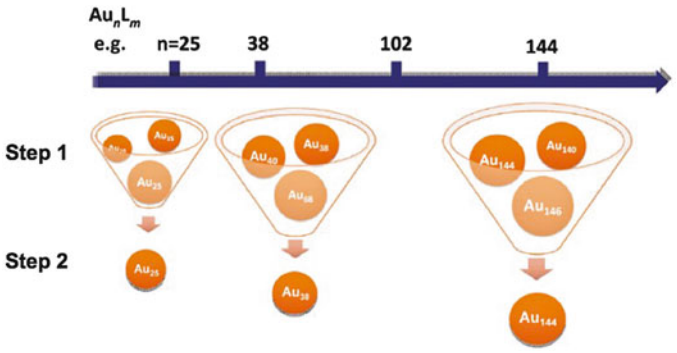

Fig. 3 Size-focusing methdology for the synthesis of atomically preciese gold nanoclusters. First step: control over size range; second step: size "focusing" into single-size product. By shifting the initial size range, different-sized nanoclusters are obtained. Adapted with permission from [37]

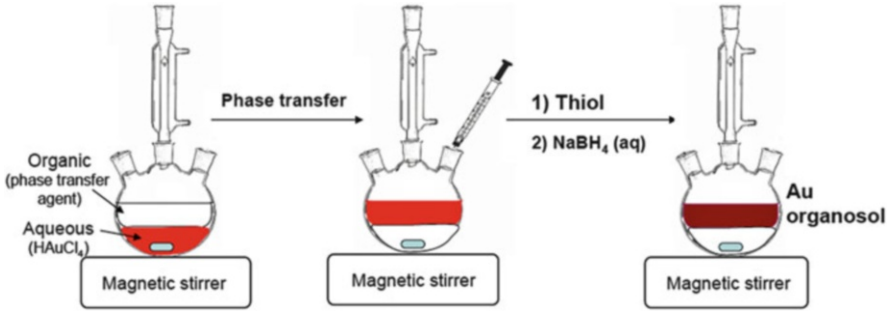

Fig. 4 Two-phase synthesis method of gold nanoclusters

A key to select one particular size of gold nanoclusters in the size-focusing methodology is to control the distribution of the starting nanoclusters in a proper size range (Fig. 3). If the size range of the starting nanoclusters is too wide, several stable species may be resulted after size focusing, which necessitates difficult post-synthetic separation. Control over the initial size distribution can be achieved through adjusting the reaction parameters such as gold to thiol ratio, solvent, ligand's bulkiness, and growth kinetics.

In the two-phase synthesis of thiolate-protected gold nanoclusters, four reagents are needed: the gold salt ($HAuCl_4$), phase transfer agent ((n-$C_8H_{17})_4NBr$, denoted as TOAB), protecting ligand (thiol), and reducing agent ($NaBH_4$). In a typical synthesis (Fig. 4), gold salt and phase transfer agent are first dissolved in water and toluene, respectively. Under the help of phase transfer agent TOA^+, the gold salt $[AuCl_4]^-$ is transferred from the aqueous phase to the toluene phase. Then thiol is added. The thiol reduces Au(III) into Au(I) to form colorless Au(I)-SR complexes or polymers. Then the reducing agent is added to reduce the Au(I) complex/polymer into gold nanoclusters protected by thiolate. The as-obtained gold nanoclusters are polydispersed, and they should be further subjected to size focusing in the presence of excess thiol and often at high temperature.

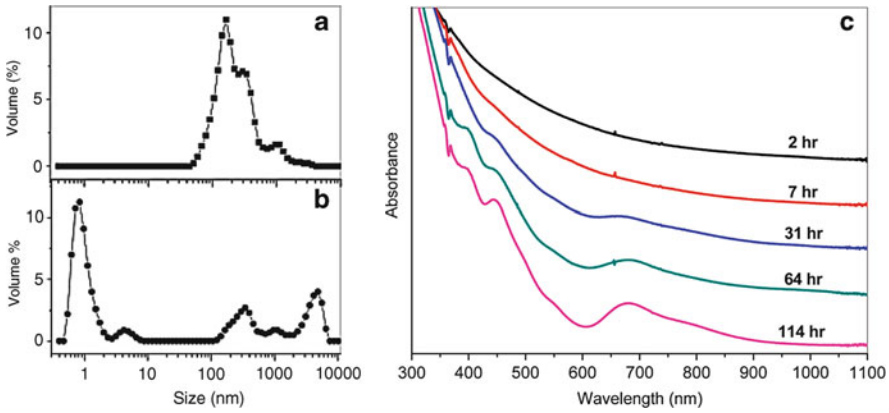

Fig. 5 Size-focusing synthesis of $Au_{25}(SC_2H_4Ph)_{18}$ nanoclusters. (**a**) and (**b**) Dynamic light scattering (DLS) characterization of Au(I)-SR intermediate in the form of aggregates (prepared with and without kinetic control, respectively); (**c**) evolution of the optical spectrum of the crude product with aging time in the presence of excess thiol. Adapted with permission from [38, 62]

Below we illustrate how to tune the initial size range by adjusting the reaction conditions to finally obtain pure gold nanoclusters with well-defined compositions, e.g. $Au_{25}(SC_2H_4Ph)_{18}$, $Au_{38}(SC_2H_4Ph)_{24}$, $Au_{144}(SC_2H_4Ph)_{60}$, and $Au_{333}(SC_2H_4Ph)_{79}$.

4.1.1 The Case of $Au_{25}(SR)_{18}$

Among the reported well-defined $Au_n(SR)_m$ nanoclusters capped by thiolates (*n* and *m* refer to the numbers of gold atoms and thiolate ligands, respectively), the 25-atom $Au_{25}(SR)_{18}$ nanocluster is perhaps the most extensively studied one [3], probably due to its ubiquitous nature in various syntheses. The reported, high yielding synthetic methods include size-conversion [42], two-phase and one-phase methods [38, 62].

In the two-phase synthesis, the size control was performed through kinetic control of the size of the initially formed Au(I)-SR complexes (or polymers). It was found that when mixing gold salt and PhC_2H_4SH thiol under conditions of *0°C and slow stirring*, the subsequent reduction Au(I)-SR (here R = C_2H_4Ph) by $NaBH_4$ and aging resulted in very pure $Au_{25}(SC_2H_4Ph)_{18}$ with high yield [38]. The preliminary study for the high yielding synthesis of $Au_{25}(SC_2H_4Ph)_{18}$ indicated that, under the low temperature and slow stirring conditions, the Au(I)-SR complex grew into aggregates with a unimodal distribution of size about 100–300 nm (Fig. 5a), while without kinetic control the Au(I)-SR complex aggregated randomly (Fig. 5b). The size range of the Au(I)-SR aggregates was found to be quite important for the exclusive formation of $Au_{25}(SC_2H_4Ph)_{18}$ nanoclusters via size focusing, evidenced by the appearance of distinct optical absorption peaks in the crude product's spectrum characteristic of $Au_{25}(SR)_{18}$ nanoclusters [38].

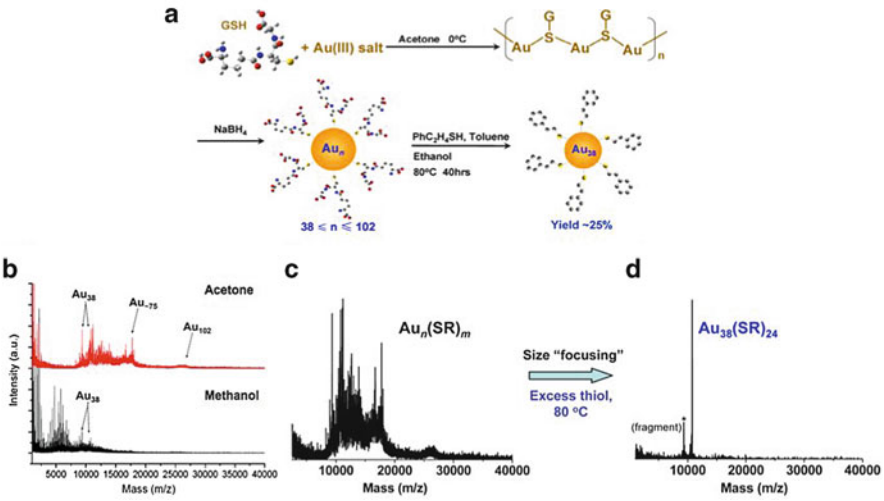

Fig. 6 (**a**) Scheme of the size-focusing synthesis of $Au_{38}(SR)_{24}$ nanoclusters; (**b**) the effect of solvent on the size range of the initial crude gold nanoclusters; (**c**, **d**) illustrate size focusing of polydispersed nanoclusters into pure $Au_{38}(SR)_{24}$. Adapted with permission from [39]

This was indeed the first high yielding synthesis of $Au_{25}(SR)_{18}$ nanoclusters (yield: 40–50%, Au atom basis). Recent work by Liu et al. further demonstrated the importance of controlling Au(I)-SR for the product size [63].

For the one-phase synthesis of $Au_{25}(SC_2H_4Ph)_{18}$, THF was used as the solvent to dissolve reactants $HAuCl_4$, PhC_2H_4SH, and TOABr. After reduction by $NaBH_4$ and spontaneous size focusing in the presence of excess thiol, pure $Au_{25}(SC_2H_4Ph)_{18}$ was obtained [62]. Figure 5c shows the evolution of the absorption spectrum of the product, in which the initial featureless UV-vis spectrum gradually evolved into the well-defined spectrum of $Au_{25}(SC_2H_4Ph)_{18}$. The solvent was found to play an important role in controlling the size distribution of the initial gold nanoclusters [62, 63]. In the THF system, the initially formed gold nanoclusters had a size range smaller than $Au_{\sim 100}$ [64], and further aging led to size focusing of the polydispersed product into single-sized $Au_{25}(SC_2H_4Ph)_{18}$. Different thiolate-ligand-protected $Au_{25}(SR)_{18}$ nanoclusters were also attained following the size-focusing method, where R = C_nH_{2n+1}, G (glutathione), and so on [62].

4.1.2 The Case of $Au_{38}(SR)_{24}$

Another well-known gold nanocluster is the 38-gold-atom cluster protected by 24 thiolate ligands, i.e. $Au_{38}(SR)_{24}$. In the synthesis, the size range of the initial gold nanoclusters was controlled by the solvent (acetone was used) [39]. The initial gold clusters were made by a water-soluble thiol (glutathione). Gold salt was first mixed with glutathione in acetone (Fig. 6a), giving a turbid yellow solution since

glutathione cannot dissolve in acetone. The adding of $NaBH_4$ resulted in the immediate precipitation of gold nanoclusters as glutathione-protected gold nanoclusters cannot dissolve in acetone. The precipitation prevented further growth of the initially formed gold nanoclusters; hence, the size range of glutathione-capped $Au_n(SR)_m$ clusters was controlled in ~38 < n < ~100 (Fig. 6c). The solvent played an important role in this case: if the solvent acetone was replaced by methanol (Fig. 6b), then the initial size range was smaller, probably due to the higher reduction ability of $NaBH_4$ in methanol [6].

The precipitate was collected and redissolved in H_2O. Excess phenylethanethiol (in toluene) was added, forming an organic layer on the top of the H_2O layer, followed by heating to 80°C. The ligand exchange process transferred the gold nanoclusters from the aqueous phase to the toluene phase in which the size focusing occurred. Due to the narrow distribution of the initial gold clusters, $Au_{38}(SR)_{24}$ was obtained as the final, pure product since $Au_{38}(SR)_{24}$ is the most stable species within this range (Fig. 6d). The yield of $Au_{38}(SR)_{24}$ was ~25 % (Au atom basis). Later work by Qian et al. further found the importance of the thermal condition [65]; using the same polydisperse $Au_n(SR)_m$ nanoclusters size focusing at room temperature led to $Au_{25}(SR)_{18}$, while thermal size focusing gave rise to $Au_{38}(SR)_{24}$. Different thiols have been used to make $Au_{38}(SR)_{24}$ nanoclusters [66].

4.1.3 The Case of $Au_{144}(SR)_{60}$

$Au_{144}(SR)_{60}$ constitutes the dominant component in the previously reported polydisperse 29 kDa species which had been studied for a long time [47]. The previous 29 kDa clusters were obtained through solvent fractionation [47] or HPLC separation [47, 48], by which the yield was low, albeit Tsukuda and coworkers obtained pure $Au_{144}(SR)_{59}$ (R = $C_{12}H_{25}$) [48]. Of note, the one-ligand difference (c.f. $Au_{144}(SR)_{60}$) is probably due to the oxidation treatment [48] prior to ESI-MS analysis.

The size-focusing method was applied to the synthesis of $Au_{144}(SR)_{60}$ nanoclusters [40]. This time, the initial size distribution was controlled through tuning the golt salt to thiol ratio (Au/SR). By adjusting the $HAuCl_4$ to PhC_2H_4SH ratio to 1:3, the size range was controlled around 29 kDa, together with some $Au_{25}(SC_2H_4Ph)_{18}$ clusters (Fig. 7a, black profile of mass spectrum). In the size-focusing step, the crude polydispersed clusters were incubated in large amounts of thiol at 80°C, and after 24 h of size focusing pure $Au_{144}(SC_2H_4Ph)_{60}$ was obtained; of note, the initially present $Au_{25}(SC_2H_4Ph)_{18}$ clusters were thermally decomposed during the harsh size-focusing process [40]. The polydispersed clusters show a decay-like UV-vis spectrum (Fig. 7b, black); after size focusing, step-like bands were observed at 510 and 700 nm (Fig. 7b, red). Note that the MALDI-MS spectrum showed a broad peak for pure $Au_{144}(SC_2H_4Ph)_{60}$, this was due to the inevitable fragmentation for large-sized gold nanoclusters in MALDI-MS analysis. In contrast, ESI-MS characterization gave rise to intact cluster ions; thus, the precise formula weight was measured and the $Au_{144}(SC_2H_4Ph)_{60}$ formula was determined (Fig. 7c–e). Au_{144} clusters with different –SR have been reported [67].

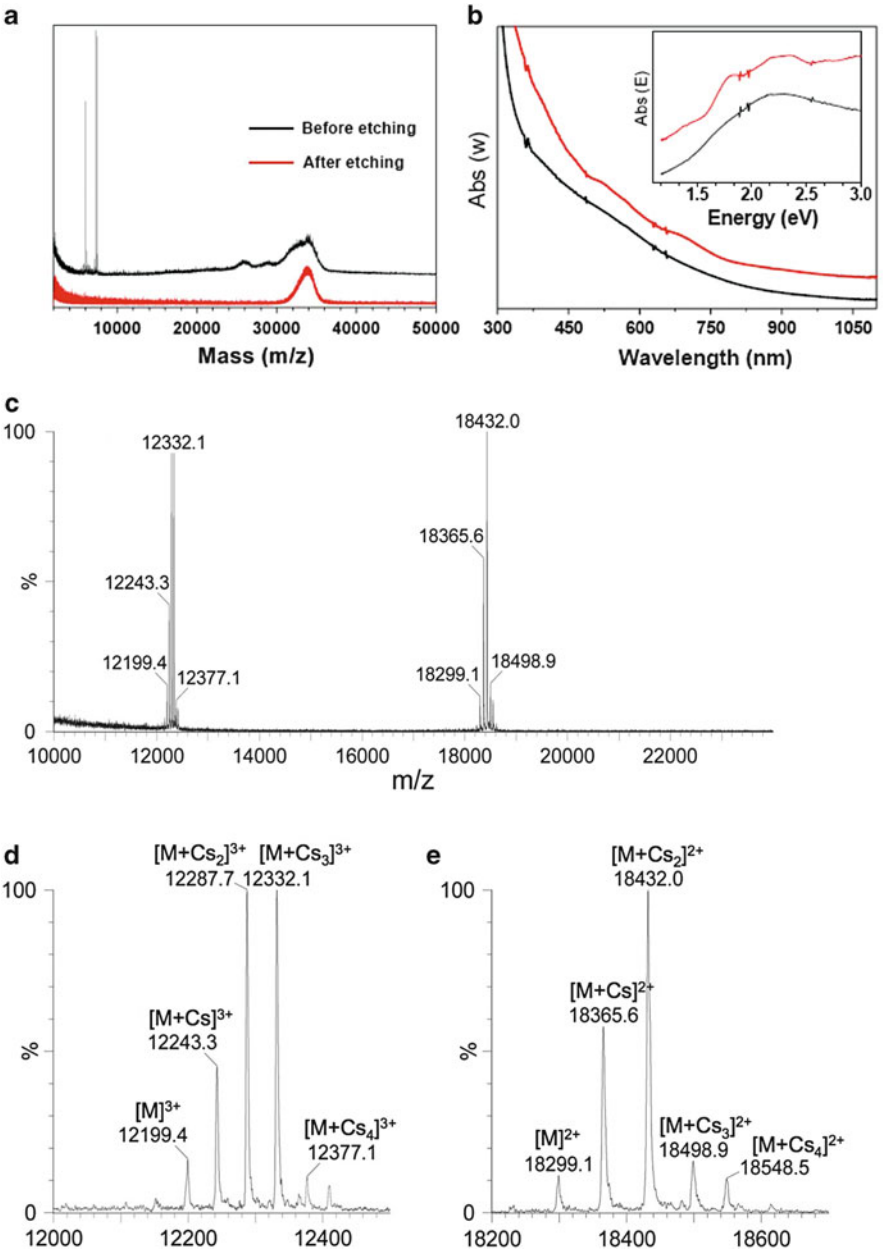

Fig. 7 Size-focusing synthesis of $Au_{144}(SC_2H_4Ph)_{60}$ nanoclusters. (**a**) MALDI of initial and final products of the size-focusing step, (**b**) UV-vis spectra of the initial and final products, (**c**) ESI-MS spectrum, and (**d**) and (**e**) zoom-in peaks (CsOAc was mixed with the clusters to form positively charged adducts for ESI detection). Adapted with permission from [40]

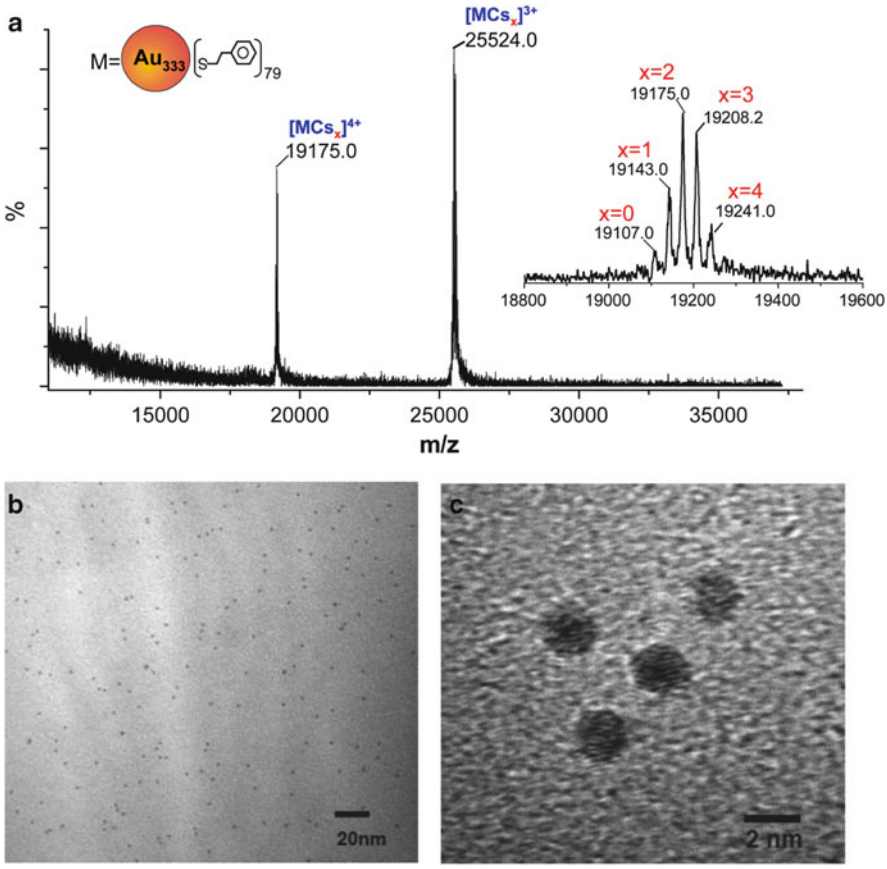

Fig. 8 (**a**) ESI-MS and (**b**) HR-TEM of the $Au_{333}(SC_2H_4Ph)_{79}$ nanoclusters. The *inset* of (**a**) shows the ($M + Cs_x$) adducts. Adapted with permission from [41]

4.1.4 The Case of $Au_{333}(SR)_{79}$

The size-focusing method was extended to the largest ever $Au_{333}(SR)_{79}$ nanocluster [41]. The synthetic protocol of this 2.2 nm atomically precise nanocluster is similar to the case of $Au_{144}(SR)_{60}$. Both cluster precursors were made through the two-phase method, with a major difference in the $HAuCl_4$ to PhC_2H_4SH ratio (i.e., 1:2 in the case of $Au_{333}(SR)_{79}$, instead of 1:3 in $Au_{144}(SR)_{60}$). Figure 8 shows a comparison of ESI-MS and TEM characterization of $Au_{333}(SR)_{79}$ nanoclusters. This giant nanocluster approaches the current detection limit of ESI-MS. New methods should be developed in future work to cope with giant nanoclusters of larger size.

4.2 Other Methods for Atomically Precise Gold Nanoclusters

Besides the ubiquitous $Au_{25}(SR)_{18}$, $Au_{38}(SR)_{24}$, $Au_{144}(SR)_{60}$, and $Au_{333}(SR)_{79}$ nanoclusters, there are increasingly more formulas of atomically precise gold nanoclusters discovered in other works, for example, $Au_{15}(SR)_{13}$, $Au_{18}(SR)_{14}$, $Au_{19}(SR)_{13}$, $Au_{20}(SR)_{16}$, $Au_{24}(SR)_{20}$, $Au_{28}(SR)_{20}$, $Au_{36}(SR)_{24}$, $Au_{40}(SR)_{24}$, $Au_{55}(SR)_{31}$, $Au_{67}(SR)_{35}$, $Au_{102}(SR)_{44}$, $Au_{130}(SR)_{50}$, and $Au_{187}(SR)_{68}$, etc. [4, 11, 12, 49–54, 68–72]. These gold nanoclusters were obtained by different methods.

4.2.1 Post-synthetic Size Separation

The $Au_{15}(SR)_{13}$, $Au_{18}(SR)_{14}$, $Au_{40}(SR)_{24}$, $Au_{55}(SR)_{31}$, $Au_{67}(SR)_{35}$, $Au_{130}(SR)_{50}$, and $Au_{187}(SR)_{68}$ were obtained through post-synthetic size separation step from a mixture of clusters [4, 49–54]. The separation methods such as HPLC, solvent fractionation, and polyacrylamide gel electrophoresis (PAGE) were successfully applied to the separation of gold nanoclusters. The separation is mainly based on the difference in solubility, size, charge state, and other factors among the nanoclusters.

4.2.2 Kinetic Control

Some nanoclusters were obtained through kinetic control, such as $Au_{19}(SR)_{13}$, $Au_{20}(SR)_{16}$, and $Au_{24}(SR)_{20}$ [60, 68, 69]. These clusters were all made by two-phase protocols, with the main difference in the reduction step. For the synthesis of $Au_{19}(SR)_{13}$, a weak-reducing agent borane-tert-butylamine $(CH_3)_3NH_2$-BH_3 (instead of $NaBH_4$) was used to reduce the Au(I)-SR complex, and it was found that the weak-reducing agent plays a key role in obtaining $Au_{19}(SR)_{13}$ [60]. If $NaBH_4$ was used, $Au_{25}(SR)_{18}$ would be the final product; hence, the rate of reduction from Au(I) to Au(0) is important for controlling the final cluster size. Controlling the reduction rate also gave rise to $Au_{20}(SR)_{16}$ [68]. In this case, small amount of $NaBH_4$ (1 equivalent per $HAuCl_4$) was drop-wise added over a 30-min period to reduce the Au(I)SR complex, instead of 10 equivalent of $NaBH_4$ poured into the reaction mixture all at once to synthesize $Au_{25}(SR)_{18}$. For the $Au_{24}(SR)_{20}$, the protocol was the same with $Au_{20}(SR)_{16}$, with the only difference in controlling the reduction process of Au(III) to Au(I) by thiol: for $Au_{20}(SR)_{16}$, the Au(III) to Au(I) reduction was kept stationary, while for the $Au_{24}(SR)_{20}$, the reduction process was kept at a slow stirring speed [69]. The glutathione-protected $Au_{15}(SR)_{13}$ and $Au_{18}(SR)_{14}$ were separated in early work [4] but recently have been individually synthesized through kinetic control [72, 73]. All these examples demonstrate the importance of kinetic control (including the reduction speed, the Au(I)-SR complex form, the type of reducing agent, the amount of reducing agent and adding speed, as well as pH if aqueous solution) in obtaining different-sized gold nanoclusters.

4.2.3 Size Conversion

Very recently, a new ligand-exchange-induced "size-conversion" method has been discovered [11, 12], which may become another universal synthetic methodology for atomically precise nanoclusters other than the size-focusing methodology. The size-conversion method allows one to expand the potpourri or size library of gold nanoclusters. It was found that the structure of the thiolate ligands plays an important role in controlling the size and structure of gold nanoclusters. For example, $Au_{28}(SPh\text{-}t\text{-}Bu)_{20}$ nanoclusters were obtained through ligand exchange of $Au_{25}(SC_2H_4Ph)_{18}$ with the 4-*tert*-butylbenzenethiol (HSPh-*t*-Bu), and similarly $Au_{36}(SPh\text{-}t\text{-}Bu)_{24}$ were obtained through ligand exchange of $Au_{38}(SC_2H_4Ph)_{24}$ [11, 12]. This size-conversion methodology is very effective, with yields larger than 90% in both cases. Mechanistic studies on the $Au_{38}(SC_2H_4Ph)_{24}$ to $Au_{36}(SPh\text{-}t\text{-}Bu)_{24}$ conversion show that the size and structure conversion process was triggered by the geometric bulkiness of –SPh-*t*-Bu thiolate [74]. Based on this size-conversion strategy, a series of *new* sizes of nanoclusters may be obtained in future work using well-defined nanoclusters as the starting materials (as opposed to gold salt as the starting material in direct synthesis).

5 Structures of Gold Nanoclusters

The great progress made in obtaining large amounts of atomically precise gold nanoclusters has led to successful crystallization and structure determination of some of the nanoclusters discussed above. The atomic structures of gold nanoclusters reveal how the gold atoms are assembled in a specific-size metal core and how the surface is protected by ligands. The recent progress in crystallization of gold nanoclusters starts to uncover the mystery and the beauty of nanoclusters [7–12]. Through single-crystal X-ray diffraction, the position of each gold atom in a gold nanocluster can be unambiguously pinned down. The gold atoms of a nanocluster indeed assemble into a variety of highly ordered geometric structures with various symmetries. One would be quite amazed that nature could find so many simple yet elegant ways to assembly atoms into highly stable, versatile structures. It is the versatility of structures of gold nanoclusters that makes the nanocluster research particularly appealing.

Besides the core structure in a ligand-protected gold nanocluster, the surface structure is also of major importance for understanding what determines the stability of the nanocluster. On the surface of the symmetric metal core, nature finds unique ways to arrange the surface ligands for each metal core structure in order to protect the core well. Owing to the specific chemistry between organic ligand and gold, nanoclusters with different types of ligands may have different bonding rules, as different types of organic ligands have different metal–ligand coordination modes, which are reflected in the surface structure of metal nanoclusters. For example,

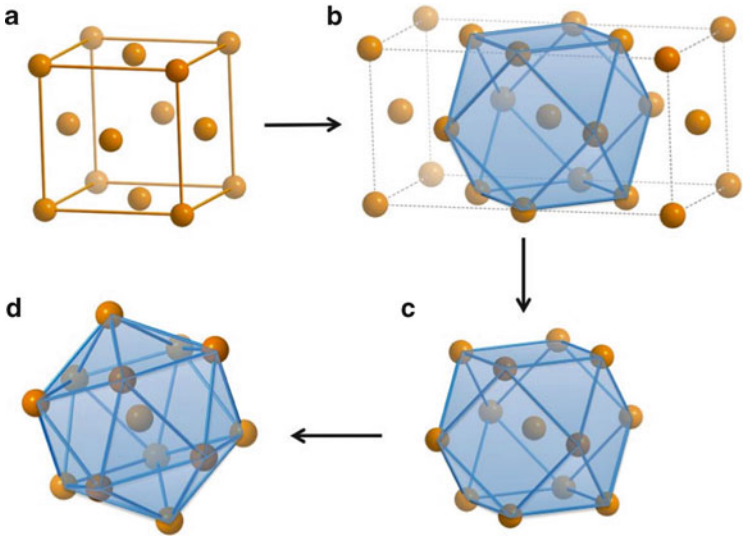

Fig. 9 (**a**) FCC unit cell; (**b** to **c**) construction of cuboctahedron from FCC; (**d**) icosahedron transformed from cuboctahedron by corrugating the middle 6-atom (Au_6) hexagon into a chair-like configuration

phosphine ligands tend to simply adsorb on the surface gold atoms via a one-on-one fashion (terminal bonding) [16–29], while thiolate ligands often form a chain-like structure by incorporating some gold atoms [7–13, 75–81]. The so far revealed surface structure modes [7–13] of gold nanoclusters provide valuable information on how the larger nanoclusters should be stabilized by the thiolate ligand and what factors determine their stability.

The reported structures of thiolate-protected gold nanoclusters can be categorized into FCC and non-FCC types (where FCC: face-centered cubic) [7–13]. Bulk gold adopts an FCC structure (Fig. 9a), and its unit cell comprises 8 vertices and 6 face centers. The 14-atom FCC unit cell is an empty structure (i.e., non-centered), from which a cuboctahedron consisting of 13 atoms can be readily constructed (Fig. 9b). The cuboctahedron is faceted by 6 squares and 8 triangles, and the center atom is coordinated to 12 first-shell atoms. Transformation of the 13-atom cuboctahedron gives rise to a 13-atom icosahedral structure (Fig. 9c, d) [82], which preserves the 12 coordination but the surface becomes exclusively triangular facets (Fig. 9d). Overall, the cuboctahedron is a fragment of FCC, but the icosahedron is not, as the presence of fivefold rotation axis in the icosahedron breaks the cubic symmetry.

Below we first discuss the non-FCC-type structures with increasing size, including $Au_{25}(SC_2H_4Ph)_{18}$, $Au_{38}(SC_2H_4Ph)_{24}$, and $Au_{102}(SPh\text{-}COOH)_{44}$ [7–10]. Examples of FCC structures include $Au_{28}(S\text{-}Ph\text{-}t\text{-}Bu)_{20}$ and $Au_{36}(S\text{-}Ph\text{-}t\text{-}Bu)_{24}$ [11, 12].

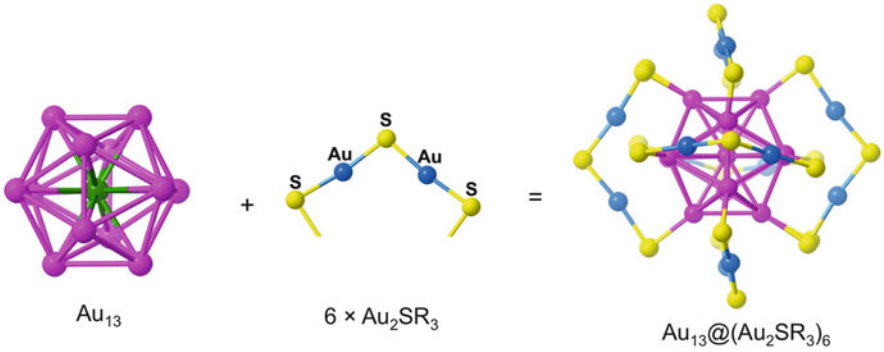

Fig. 10 Total structure of $Au_{25}(SC_2H_4Ph)_{18}$. The carbon tails ($-SC_2H_4Ph$) are omitted for clarity

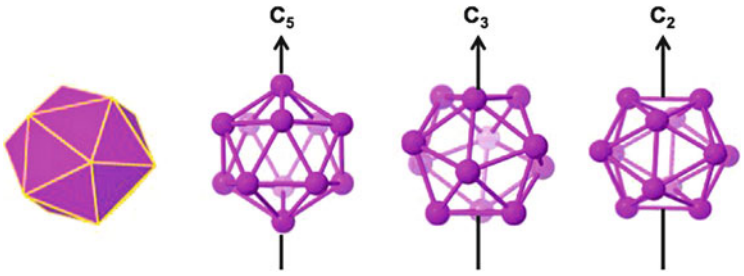

Fig. 11 Symmetry of an icosahedron (the center is removed for clarity)

5.1 Non-FCC Structures of Gold Nanoclusters

5.1.1 The Case of $Au_{25}(SC_2H_4Ph)_{18}$

The $Au_{25}(SC_2H_4Ph)_{18}$ nanocluster possesses a quasi-spherical structure and may be viewed as a kernel-shell structure [8, 9]. A unique feature in thiolate-protected gold nanoclusters is that not all the gold atoms are in the kernel; instead, some gold atoms are incorporated into the ligand shell to protect the kernel. For other organic ligands in the protected gold nanoclusters such as phosphine, simple adsorption bonding mode is seen, and the gold atoms in the formula are all located in the kernel.

There are 13 gold atoms in the kernel of $Au_{25}(SC_2H_4Ph)_{18}$; these 13 gold atoms assemble into a highly symmetric icosahedron, with one gold atom in the center and 12 gold atoms on the 12 vertices of the icosahedron (Fig. 10). The central gold atom forms 12 radial bonds with the outside 12 gold atoms, hence the coordinate number of the central atom is 12, identical with that of bulk gold.

Among the polyhedrons, the icosahedron has the highest symmetry (Fig. 11). It possesses 12 vertices, 30 edges, and 20 equal-lateral triangular faces. It can be viewed as 20 radially packed tetrahedrons sharing a common vertex and three facets

with neighboring tetrahedrons. Six five-fold (C_5) rotation axes can be readily identified on each opposite pair of *vertices*, and fifteen two-fold (C_2) axes on each opposite pair of *edges*, and ten three-fold (C_3) axes on each opposite pair of *faces*. Accordingly, one can have three views of an icosahedron based on its C_2, C_3, or C_5 axis (Fig. 11). If viewed with respect to a C_2 axis, a 2-2-4-2-2 five layers of atoms can be identified (the central atom not considered). Similarly, when viewing from a C_3 axis, there are four layers of atoms 3-3-3-3, and from C_5, there are also four layers of atoms but with a 1-5-5-1 configuration.

The icosahedral Au_{13} kernel is protected by six "V-shaped" –SR-Au-SR-Au-SR–chains or oligomers (Fig. 10). This oligomeric structure is often called a staple motif, because it has two sulfur ends binding two surface gold atoms of the kernel in a way resembling a staple. Based on the number of gold atoms in the chain, there are monomeric staples, dimeric staples, and so on. For example, the six V-shaped staples in $Au_{25}(SR)_{18}$ are called dimeric staples since there are two gold atoms incorporated in the chain. In regard to the distribution of the six dimeric staples on the icosahedron, if one views from the three mutually perpendicular C_2 axes of the icosahedron (Fig. 10), two dimeric staples are seen on the top and the bottom, another two on the front and the back, and two more on the left and the right. Since six staple motifs have 12 sulfur ends, all the 12 surface gold atoms of the Au_{13} icosahedron are protected by the –SR groups. In terms of symmetry, the Au_{13} kernel has the highest I_h symmetry, but the $Au_{25}S_{18}$ skeleton reduces its symmetry to D_{2h}. Following the above anatomy, the $Au_{25}(SC_2H_4Ph)_{18}$ structure may be represented as $Au_{13}@[Au_2(SR)_3]_6$ to illustrate the kernel and the exterior shell.

It should be stressed that the staple gold atoms also interact with the gold atoms of the Au_{13} kernel via face capping, with one shorter Au–Au contact (3.02–3.12 Å) and two longer ones (3.18–3.27 Å) to the other two Au atoms on the face it is capping.

The $Au_{25}(SR)_{18}$ nanocluster can have different, stable charge states (e.g., $q = -1$, 0, +1, etc.) [13, 83–88]. The initially reported $Au_{25}(SR)_{18}$ nanocluster was negatively charged, with a positive counterion $[N(n\text{-}C_8H_{17})_4]^+$ in the unit cell. The negatively charged Au_{25} can be oxidized to neutral $[Au_{25}(SR)_{18}]^0$, and the $Au_{25}S_{18}$ framework is preserved in the neutral $[Au_{25}(SR)_{18}]^0$, with the only difference in that the $[Au_{25}(SR)_{18}]^0$ framework is less distorted than the negatively charged $[Au_{25}(SR)_{18}]^-$ [13]. The $[Au_{25}(SR)_{18}]^0$ is paramagnetic [89], while the $[Au_{25}(SR)_{18}]^-$ and $[Au_{25}(SR)_{18}]^+$ are diamagnetic [84].

5.1.2 The Case of $Au_{38}(SC_2H_4Ph)_{24}$

The $Au_{38}(SC_2H_4Ph)_{24}$ nanocluster possesses an Au_{23} kernel which is composed of two icosahedrons (building blocks) via face-sharing (Fig. 12a) [10]. If we start with one icosahedron (with two opposite triangular faces on the top and the bottom, i.e. the C_3 orientation, see Fig. 11 above), next, place the second icosahedron on the

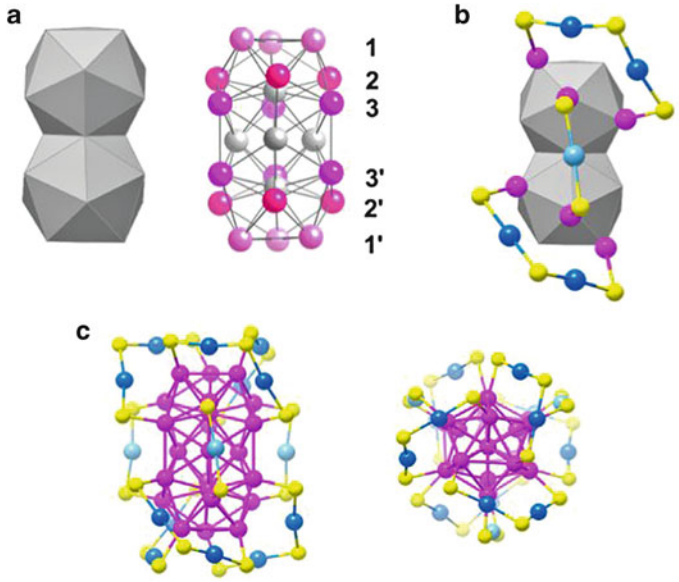

Fig. 12 Total structure of $Au_{38}(SC_2H_4Ph)_{24}$. The carbon tails ($-SC_2H_2Ph$) are omitted for clarity. (**a**) Au_{23} biicosahedral kernel. (**b**) Position of dimeric staples [$Au_2(SR)_3$] and monomeric staple [$Au(SR)_2$]. (**c**) *Side view* and *top view* of the $Au_{38}(SR)_{24}$ total structure. Color labels: *yellow* = sulfur, *other colors* = gold

top of the first one via sharing a triangular face, we obtain a rod-like biicosahedron structure (Fig. 12a). When counting the number of atoms, there are $13 + 13 - 3 = 23$ in this face-sharing biicosahedral structure; of note, face-sharing consumes 3 atoms. This Au_{23} kernel has a D_{3h} symmetry. Among the 23 atoms, 2 atoms are in the icosahedral centers, 3 atoms are used for face-sharing; hence, only 18 atoms are exposed and need protection by thiolate groups.

The 18 surface gold atoms on the biicosahedral kernel are protected by 9 staple motifs, with 3 of them being monomeric staples (–SR-Au-SR–), and the remaining 6 motifs being dimeric staples (–SR-Au-SR-Au-SR–). If viewed from the C_3 axis of the biicosahedral kernel, the 18 surface atoms can be divided into 6 layers (1–3 and mirror imaged 1′–3′, Fig. 12a). Three dimeric staples are located on the top icosahedron, with one end of each dimeric staple pinning down to the atom on layer 1, while the other end pining down on layer 3 (Fig. 12b). The rotary arrangement of the three dimeric staples along the C_3 axis resembles the tri-blades of a fan or propeller [10] (Fig. 12c). The remaining three dimeric staples are located on the bottom icosahedron with the same rotation direction. The three monomeric staples are located on the waist of the biicosahedral kernel, connecting the atoms on the layer 2 and 2′ together, reinforcing the connection between the two icosahedra. The protecting staples reduce the D_{3h} symmetry of the Au_{23} biicosahedral kernel to the D_3 symmetry of the overall $Au_{38}S_{24}$. Similar to the

anatomy of $Au_{25}(SR)_{18}$, the formula of $Au_{38}(SR)_{24}$ may be written as $Au_{23}@[Au(SR)_2]_3[Au_2(SR)_3]_6$, which indicates that Au_{38} nanocluster has a 23-gold-atom kernel protected by three monomeric staples and six dimeric staples.

The $Au_{38}(SR)_{24}$ structure is chiral, as reflected from the rotating arrangement of the dimeric staples. The unit cell of $Au_{38}(SR)_{24}$ nanoclusters indeed contains a pair of enantiomers. The dimeric staples can be arranged in a left-handed or right-handed way, forming two enantiomers of the Au_{38} nanocluster.

5.1.3 The Case of $Au_{102}(SPh\text{-}COOH)_{44}$

$Au_{102}(SR)_{44}$ was the first reported structure of thiolate-protected gold nanoclusters [7]. Its formula may be written as $Au_{79}@[Au(SR)_2]_{19}[Au_2(SR)_3]_2$. The Au_{102} nanocluster possesses a 79-gold-atom kernel. To understand the Au_{79} kernel, we first briefly discuss Marks' decahedron and rhombicosidodecahedron – which are important noncrystalline shapes.

The Marks' decahedron was discovered in early research on the multi-twinned nanoparticles. L. D. Marks found that a special form of decahedron is one of the common low-energy (i.e., stable) shapes for small nanoparticles [90, 91]. A decahedron can be viewed as five tetrahedrons assembled together by sharing a common edge (as the central axis), with each tetrahedron sharing two facets with neighboring tetrahedrons, hence forming a fivefold twinned structure (Fig. 13a). The remaining two facets of each tetrahedron are exposed, composing the total 10 triangular {111} surfaces of the decahedron. By truncating through the five horizontal edges of a decahedron, one obtains an Ino decahedron with additional five {100} facets (Fig. 13b). A Marks' decahedron is a derivative of Ino's decahedron. Marks found that when introducing a reentrant {111} surface at each of the five vertical edges of Ino's decahedron, a more stable decahedron structure can be obtained (Fig. 13c). A Marks' decahedron is denoted by (m, n, p), with m indicating the number of atoms on the equatorial edges, n the number of atoms on the vertical edge, and p the number of atoms on the reentrant edge (Fig. 13d) [44].

The central portion of the Au_{79} kernel of $Au_{102}(SR)_{44}$ is actually a 49-atom Marks' decahedron of (2,1,2). The 49 atoms can be counted as $4 \times 1 + 3 \times 5 + 2 \times 10 + 1 \times 10 = 49$, indicating that there are four atoms at the central axis, 3 atoms at the first pentagon column, 2 atoms on the second, and 1 atom on the third (Fig. 13e).

The Au_{49} Marks' decahedron has *ten* extended {111} facets. In order to reduce the exposed surface area, nature chooses to cover each {111} facet with *three* more atoms (Fig. 14a), giving rise to Au_{79}. The three additional atoms adopt close packing onto the Au_9 triangular {111} facets; hence, there are additional 15 gold atoms on the top of the Au_{49} decahedron and another 15 on the bottom (Fig. 14b), composing an Au_{79} kernel (Fig. 14c). The 15 atoms actually connect together to

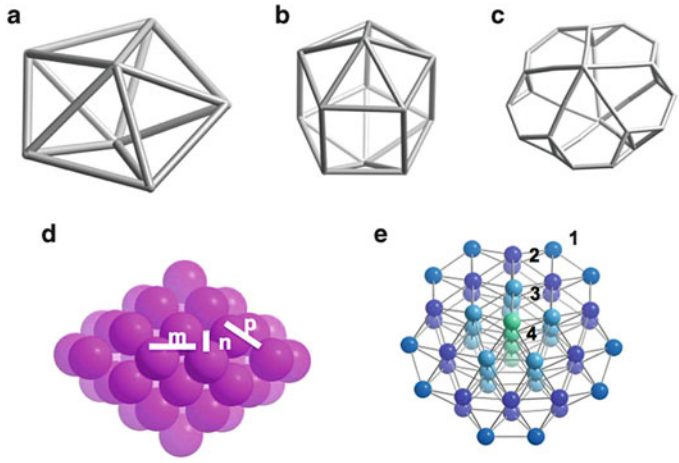

Fig. 13 (**a**–**c**) From decahedron to Ino's decahedron to Marks' decahedron; (**d**) *side view* of a 49-atom Marks' decahedron with (m, n, p) = (2, 1, 2); (**e**) C_5-axis tilted view of a 49-atom Marks' decahedron with numbers indicating the number of atoms in a column

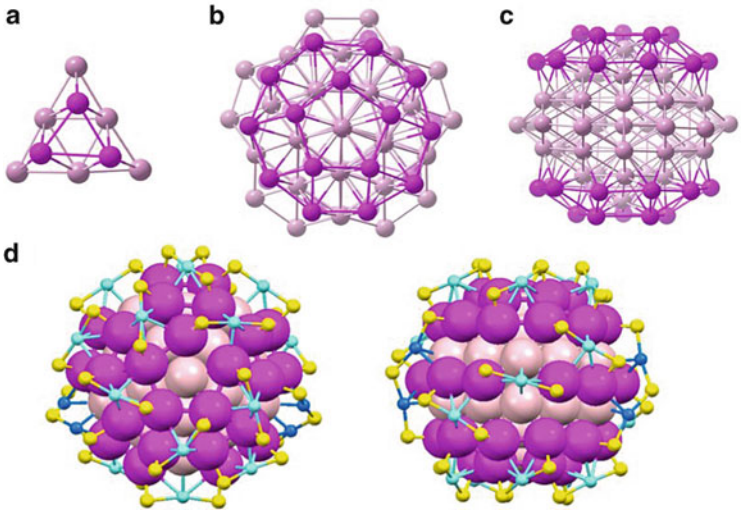

Fig. 14 Total structure of $Au_{102}(SPh\text{-}p\text{-}COOH)_{44}$. The carbon tails (–Ph-*p*-COOH) are omitted for clarity: (**a**–**c**) construction of Au_{79} kernel from Au_{49} Marks' decahedron by face capping; (**b**) *top view* and *side view* of $Au_{102}(SR)_{44}$. Color labels: *yellow* = sulfur, *other colors* = gold

form an umbrella-like structure to cover the top or bottom of the Marks' decahedron (Fig. 14b). It has a pentagon as the central part of the cap (Fig. 14b), five triangles and five squares which surround the pentagon. The two 15-atom caps are actually part of a rhombicosidodecahedron [92].

The addition of the two cap structures to the Marks' Au_{49} decahedron makes the kernel more vertex-exposing, instead of face-exposing. By doing so, the kernel provides more footholds for the thiolate staples to anchor on the surface. Together with the 10 atoms on the equator of the Marks' decahedron, there are 40 atoms total exposed on the surface. Each monomeric staple (–SR-Au-SR–) binds to a square of the rhombicosidodecahedron cap (Fig. 14d). Hence, there are 5 monomeric staples on the top of the 79-atom kernel and another 5 on the bottom. The other 9 monomeric staples together with 2 dimeric staples are distributed on the waist of the kernel. Of note, $Au_{102}(SR)_{24}$ is chiral due to the rotary arrangement of the staples.

5.2 FCC Structures

The prevalence of icosahedral structures in nanoclusters led researchers to conclude that FCC structures would not exist in gold-thiolate nanoclusters. However, recent work by Zeng et al. has successfully attained two FCC-structured nanoclusters, including Au_{28}(SPh-*t*-Bu)$_{20}$ and Au_{36}(SPh-*t*-Bu)$_{24}$ [11, 12]. This breaks the earlier thought that non-FCC icosahedral structures would be more stable than FCC-related cuboctahedral structures [44].

5.2.1 The Case of Au_{28}(SPh-*t*-Bu)$_{20}$

The Au_{28}(SPh-*t*-Bu)$_{20}$ nanocluster was converted from $[Au_{25}(SC_2H_4Ph)_{18}]^-TOA^+$ (where TOA = $^+N(n\text{-}C_8H_{17})_4$) by reaction with excess 4-*tert*-butylbenzenethiol (HSPh-*t*-Bu, TBBT) at 80°C [12]. Interestingly, the structure of $Au_{28}(SR)_{24}$ is significantly different from that of $Au_{25}(SR)_{18}$. The $Au_{28}(SR)_{20}$ nanocluster possesses a cuboctahedron-based kernel, while the kernel of $Au_{25}(SR)_{18}$ is an icosahedron.

$Au_{28}(SR)_{20}$ has a rod-like Au_{20} kernel, which is composed of two interpenetrating cuboctahedra (Fig. 15a, c) [12]. The two cuboctahedra share six gold atoms; hence, the number of gold atoms in the kernel is 13 + 13 − 6 = 20. This Au_{20} kernel can be viewed as a fragment of the bulk FCC structure. It exhibits layer-by-layer atomic planes; Fig. 15b indicates {111} planes marked as **a**-**b**-**c**. Besides, the Au_{20} kernel is enclosed by well-defined crystal planes: four isosceles-trapezoid-shaped {111} facets on the front and back (Fig. 15d, blue shadowed) and two rectangular-shaped {100} faces on the top and bottom (Fig. 15d, yellow shadowed). The Au_{20} kernel adopts quasi-D_{2h} symmetry.

The thiolate-protecting modes in the $Au_{28}(SR)_{20}$ structure comprise two types. First, four dimeric staples protecting the four {111} facets on the front and back sides of the Au_{20} rod, arranged in a rotating fashion (Fig. 16a). Besides, eight simple bridging thiolates can be identified, each residing on an edge of a square (i.e. {100} facet), as shown in Fig. 16b. The bridging thiolate mode was first identified in the FCC-based Au_{36}(SPh-*t*-Bu)$_{24}$ (vide infra) [11], and seems to be unique in the FCC

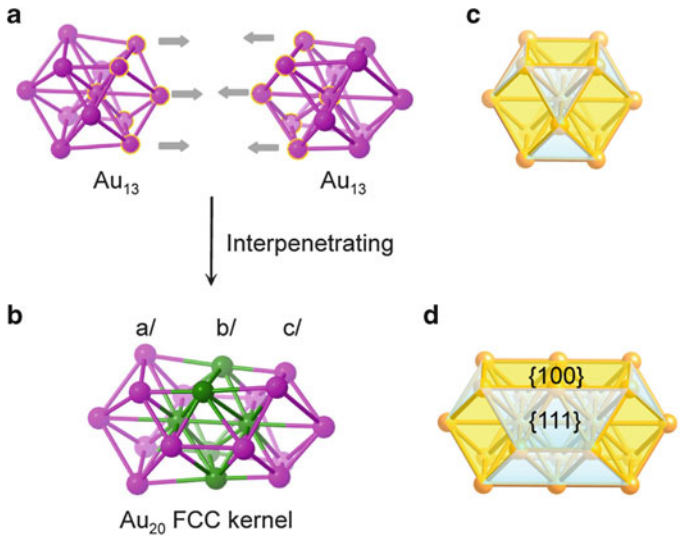

Fig. 15 (**a**, **b**) The Au_{20} kernel structure in $Au_{28}(SPh\text{-}t\text{-}Bu)_{20}$; (**c**, **d**) models of cuboctahedron and interpenetrated bicuboctahedron [12]

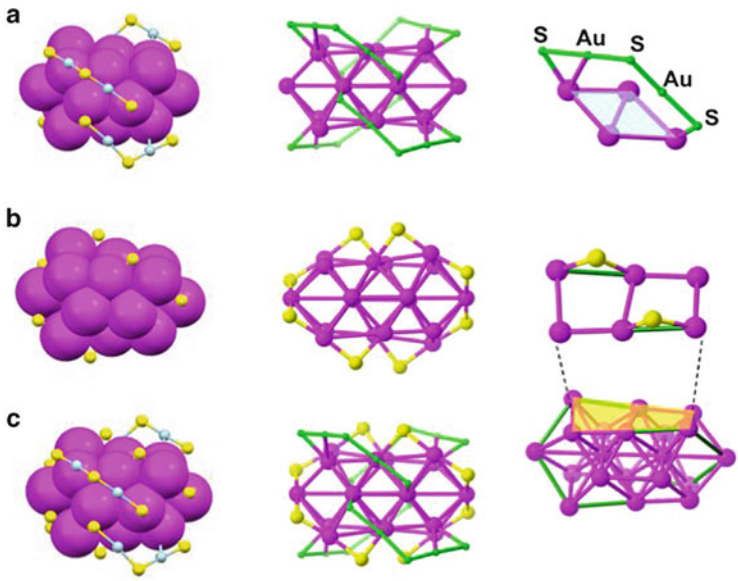

Fig. 16 Thiolate-binding modes in $Au_{28}(SPh\text{-}t\text{-}Bu)_{20}$: (**a**) dimeric staples (total: four); (**b**) bridging thiolates (total: eight); (**c**) overall $Au_{28}S_{20}$ framework. (Color labels: *magenta* = Au atoms in the kernel, *blue* = Au in dimeric staples, *yellow* = sulfur, the four dimeric staples are highlighted in *green* in panels **a** and **c**)

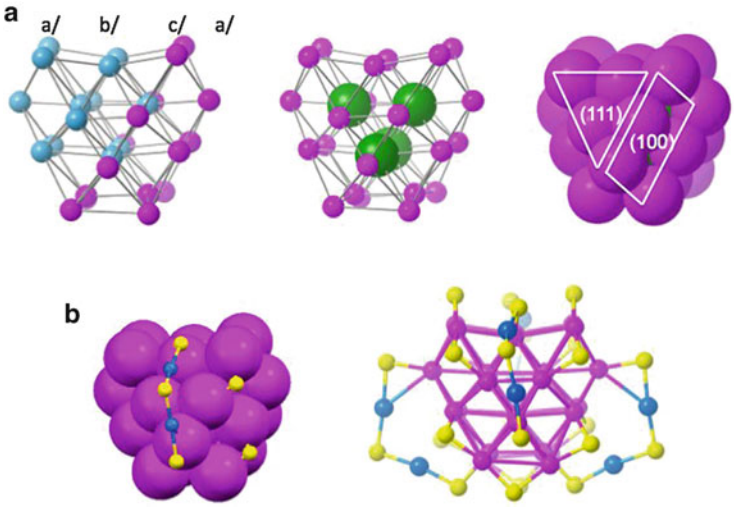

Fig. 17 Total structure of $Au_{36}(SPh\text{-}t\text{-}Bu)_{24}$. The carbon tails (–Ph-*t*-Bu) are omitted for clarity. (**a**) The view of kernel structure based on polyhedron fusion and shell-by-shell mode, respectively. (**b**) Surface thiolate-protecting modes and the total structure of $Au_{36}(SR)_{24}$ [11]. Color labels: *yellow* = sulfur, all the *other colors* are gold atoms

structure. The overall structure of $Au_{28}(SR)_{20}$ has a quasi-D_2 symmetry (Fig. 16c). The formula of $Au_{28}(SR)_{20}$ may be represented as $Au_{20}[Au_2(SR)_3]_4(SR)_8$. Note that the structure of $Au_{28}(SR)_{20}$ is also chiral as the case in $Au_{38}(SR)_{24}$ and $Au_{102}(SR)_{44}$, due to the rotation arrangement of the dimeric staples and bridging thiolates. A pair of enantiomers exists in the unit cell of the $Au_{28}(SR)_{24}$ single crystals.

5.2.2 The Case of $Au_{36}(SPh\text{-}t\text{-}Bu)_{24}$

The $Au_{36}(SPh\text{-}t\text{-}Bu)_{24}$ nanocluster was converted from $Au_{38}(C_2H_4Ph)_{24}$ by reaction with excess HSPh-*t*-Bu at 80°C [11]. It has a 28-gold-atom kernel. Unlike the icosahedron-based kernel in the $Au_{38}(SR)_{24}$ nanocluster, the 28-gold-atom kernel in Au_{36} is based on cuboctahedral building blocks and thus can be viewed as a fragment of the FCC structure. From the view of polyhedron fusion, the Au_{28} kernel is composed of four interpenetrating cuboctahedra, with two cuboctahedra on the top, the other two on the bottom (Fig. 17a). The four center atoms of the four cuboctahedra assemble into a tetrahedron. The other way to appreciate the kernel is to view it as a two-shelled structure. In the center of Au_{28} kernel, four gold atoms pack into an Au_4 tetrahedron. Onto each facet of the Au_4 tetrahedron, a six-atom Au_6 triangle is close-packed. Hence, there are 24 gold atoms on the second shell, forming a vertex/edge-truncated tetrahedron. Since this Au_{28} kernel has an FCC structure, one can identify **a-b-c-a** cubic-close-packing layers (Fig. 17a). The Au_{28} gold kernel exposes four {111} and six {100} facets. The four {111} facets

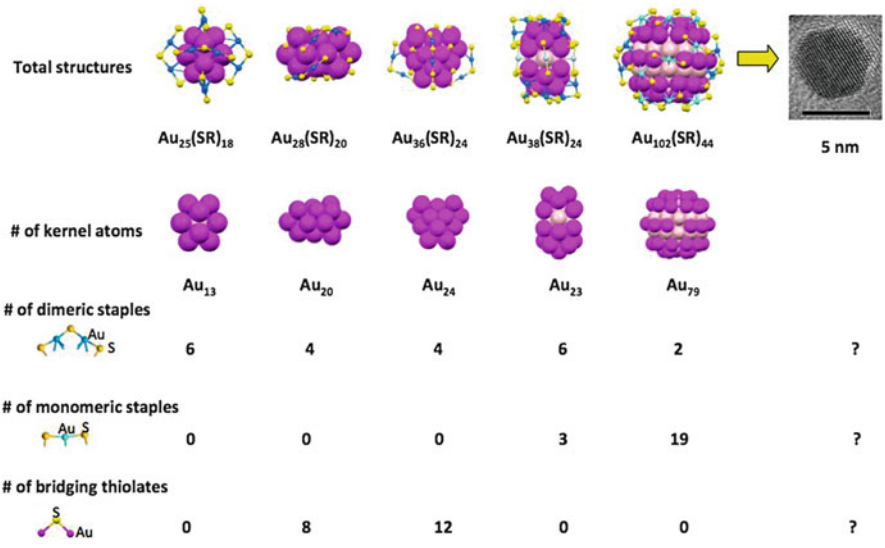

Fig. 18 Structural evolution of $Au_n(SR)_m$ nanoclusters

constitute the four faces of the truncated tetrahedral Au_{28} kernel, and six {100} facets on the six edges of the tetrahedron.

The Au_{28} kernel is protected by four dimeric staples (–SR-Au-SR-Au-SR–) and twelve bridging thiolates (–SR–). Each of the four dimeric staples protects one {111} facet (Fig. 17b). On each {100} facet (comprising two squares), two bridging thiolates can be identified (Fig. 17b). The $Au_{36}S_{24}$ framework has an overall D_{2h} symmetry and is *achiral*. With the above analysis, the formula of $Au_{36}(SR)_{24}$ may be represented as $Au_{28}[Au_2(SR)_3]_4(SR)_{12}$ to illustrate the partition of gold atoms in the kernel and surface of the cluster.

6 Summary

The above discussed nanocluster structures are summarized in Fig. 18, in which one can see the evolution or general trend of structural features with increasing size. Particularly interesting questions are: what structures in terms of kernel and staple motifs would be adopted in smaller nanoclusters ($n < 25$)? What structures would the intermediate-size ($38 < n < 102$) and larger nanoclusters ($n > 102$) exhibit? Future work is expected to reveal more structures and systematic structural rules may be formulated.

Other than the structures of nanoclusters, the electronic and optical properties of such nanoclusters remain to pursue in future work. For example, $Au_n(SR)_m$ nanoclusters are found to be fluorescent but the quantum yields are quite low (up to a few percent). What factors govern the photoluminescence properties? Is it possible to largely enhance the luminescence?

The biggest question in the field is what factors determine the stability of gold nanoclusters. As briefly discussed above, the geometric and electronic effects are two important aspects. Significant research is still needed to elucidate the stability mechanism. The electron-shell closing is not sufficient. For example, even for the well known $[Au_{25}(SR)_{18}]^-$, which has a formal electron count of 8e and thus satisfies electron-shell closing (i.e., $1S^21P^6$), and one expects that the cluster would hold the 8e tight and exhibit the least reactivity (like the Ne atom of $2s^22p^6$), but we found that $[Au_{25}(SR)_{18}]^-$ readily reacts with O_2 and loses one electron, forming $[Au_{25}(SR)_{18}]^0$ with an open electron-shell ($1S^21P^5$, i.e. radical) [13, 89]. We feel that the geometric factor is more important than the electronic factor in deciding the structural stability. Future work will shed more light on this and other major scientific questions of metal nanoclusters.

Acknowledgments We acknowledge financial support from the Air Force Office of Scientific Research under AFOSR Award No. FA9550-11-1-9999 (FA9550-11-1-0147) and the Camille Dreyfus Teacher-Scholar Awards Program.

References

1. Jin R, Cao Y, Mirkin CA, Kelly KL, Schatz GC, Zheng JG (2001) Photoinduced conversion of silver nanospheres to nanoprisms. Science 294:1901–1903
2. Jin R (2010) Quantum sized thiolate-protected gold nanoclusters. Nanoscale 2:343–362
3. Qian H, Zhu M, Wu Z, Jin R (2012) Quantum sized gold nanoclusters with atomic precision. Acc Chem Res 45:1470
4. Negishi Y, Nobusada K, Tsukuda T (2005) Glutathione-protected gold clusters revisited: bridging the gap between gold(I)-thiolate complexes and thiolate-protected gold nanocrystals. J Am Chem Soc 127:5261–5270
5. Tracy JB, Crowe MC, Parker JF, Hampe O, Fields-Zinna CA, Dass A, Murray RW (2007) Electrospray ionization mass spectrometry of uniform and mixed monolayer nanoparticles: $Au_{25}[S(CH_2)_2Ph]_{18}$ and $Au_{25}[S(CH_2)_2Ph]_{18-x}(SR)_x$. J Am Chem Soc 129:16209–16215
6. Qian H, Zhu M, Andersen UN, Jin R (2009) Facile, large-scale synthesis of dodecanethiol-stabilized Au_{38} clusters. J Phys Chem A 113:4281–4284
7. Jadzinsky PD, Calero G, Ackerson CJ, Bushnell DA, Kornberg RD (2007) Structure of a thiol monolayer-protected gold nanoparticle at 1.1Å resolution. Science 318:430–433
8. Heaven MW, Dass A, White PS, Holt KM, Murray RW (2008) Crystal structure of the gold nanoparticle $[N(C_8H_{17})_4][Au_{25}(SCH_2CH_2Ph)_{18}]$. J Am Chem Soc 130:3754–3755
9. Zhu M, Aikens CM, Hollander FJ, Schatz GC, Jin R (2008) Correlating the crystal structure of a thiol-protected Au_{25} cluster and optical properties. J Am Chem Soc 130:5883–5885
10. Qian H, Eckenhoff WT, Zhu Y, Pintauer T, Jin R (2010) Total structure determination of thiolate-protected Au_{38} nanoparticles. J Am Chem Soc 132:8280–8281
11. Zeng C, Qian H, Li T, Li G, Rosi NL, Yoon B, Barnett RN, Whetten RL, Landman U, Jin R (2012) Total structure and electronic properties of the gold nanocrystal $Au_{36}(SR)_{24}$. Angew Chem Int Ed 51:13114–13118
12. Zeng C, Li T, Das A, Rosi NL, Jin R (2013) Chiral structure of thiolate-protected 28-Gold-atom nanocluster determined by X-ray crystallography. J Am Chem Soc 135:10011–10013
13. Zhu M, Eckenhoff WT, Pintauer T, Jin R (2008) Conversion of anionic $[Au_{25}(SCH_2CH_2Ph)_{18}]^-$ cluster to charge neutral cluster via air oxidation. J Phys Chem C 112:14221–14224

14. Wu Z, Gayathri C, Gil RR, Jin R (2009) Probing the structure and charge state of glutathione-capped $Au_{25}(SG)_{18}$ clusters by NMR and mass spectrometry. J Am Chem Soc 131:6535–6542
15. Qian H, Zhu M, Gayathri C, Gil RR, Jin R (2011) Chirality in gold nanoclusters probed by NMR spectroscopy. ACS Nano 5:8935–8942
16. McPartlin M, Mason R, Malatesta L (1969) Novel cluster complexes of gold(0)-gold(I). J Chem Soc D 334–334
17. Briant CE, Theobald BRC, White JW, Bell LK, Mingos DMP, Welch AJ (1981) Synthesis and X-ray structural characterization of the centred icosahedral gold cluster compound $[Au_{13}(PMe_2Ph)_{10}Cl_2](PF_6)_3$; the realization of a theoretical prediction. J Chem Soc Chem Commun 201–202
18. Schmid G, Pfeil R, Boese R, Bandermann F, Meyer S, Calis GHM, Vandervelden WA (1981) $Au_{55}[P(C_6H_5)_3]_{12}Cl_6$ − a gold cluster of an exceptional size. Chem Ber 114:3634–3642
19. Teo BK, Shi XB, Zhang H (1992) Pure gold cluster of 1:9:9:1:9:9:1 layered structure: a novel 39-metal-atom cluster $[(Ph_3P)_{14}Au_{39}Cl_6]Cl_2$ with an interstitial gold atom in a hexagonal antiprismatic cage. J Am Chem Soc 114:2743–2745
20. Teo BK, Shi X, Zhang H (1991) Cluster of clusters. structure of a novel gold-silver cluster $[(Ph_3P)_{10}Au_{13}Ag_{12}Br_8](SbF_6)$ containing an exact staggered-eclipsed-staggered metal configuration. Evidence of icosahedral units as building blocks. J Am Chem Soc 113: 4329–4331
21. Boon KT, Hong MC, Hong Z, Huang DB (1987) Cluster of clusters: structure of the 37-atom cluster $[(p\text{-}Tol_3P)_{12}Au_{18}Ag_{19}Br_{11}]^{2+}$ and a novel series of supraclusters based on vertex-sharing icosahedra. Angew Chem Int Ed 26:897–900
22. Teo BK, Shi X, Zhang H (1993) Clusters of clusters. 25. Synthesis and structure of a new [gold-silver]-38-metal-atom cluster $[(Ph_3P)_{14}Au_{18}Ag_{20}Cl_{12}]Cl_2$ and its implications with regard to intracavity chemistry on metal cluster surfaces. Inorg Chem 32:3987–3988
23. Tran NT, Powell DR, Dahl LF (2000) Nanosized $Pd_{145}(CO)_x(PEt_3)_{30}$ containing a capped three-shell 145-atom metal-core geometry of pseudo icosahedral symmetry. Angew Chem Int Ed 39:4121–4125
24. Tran NT, Dahl LF (2003) Nanosized $[Pd_{69}(CO)_{36}(PEt_3)_{18}]$: metal-core geometry containing a linear assembly of three face-sharing centered Pd_{33} icosahedra inside of a hexagonal-shaped Pd_{30} tube. Angew Chem Int Ed 42:3533–3537
25. Mednikov EG, Ivanov SA, Slovokhotova IV, Dahl LF (2005) Nanosized $[Pd_{52}(CO)_{36}(PEt_3)_{14}]$ and $[Pd_{66}(CO)_{45}(PEt_3)_{16}]$ clusters based on a hypothetical Pd_{38} vertex-truncated ν_3 octahedron. Angew Chem Int Ed 44:6848–6854
26. Mednikov EG, Dahl LF (2008) Nanosized $Pd_{37}(CO)_{28}\{P(p\text{-}Tolyl)_3\}_{12}$ containing geometrically unprecedented central 23-atom interpenetrating tri-icosahedral palladium kernel of double icosahedral units: its postulated metal-core evolution and resulting stereochemical implications. J Am Chem Soc 130:14813–14821
27. Shichibu Y, Konishi K (2010) HCl-induced nuclearity convergence in diphosphine-protected ultrasmall gold clusters: a novel synthetic route to "Magic-Number" Au_{13} clusters. Small 6:1216–1220
28. Pettibone JM, Hudgens JW (2011) Gold cluster formation with phosphine ligands: etching as a size-selective synthetic pathway for small clusters? ACS Nano 5:2989–3002
29. Wan X-K, Lin Z-W, Wang Q-M (2012) Au_{20} nanocluster protected by hemilabile phosphines. J Am Chem Soc 134:14750–14752
30. Shichibu Y, Negishi Y, Watanabe T, Chaki NK, Kawaguchi H, Tsukuda T (2007) Biicosahedral gold clusters $[Au_{25}(PPh_3)_{10}(SC_nH_{2n+1})_5Cl_2]^{2+}$ (n = 2-18): a stepping stone to cluster-assembled materials. J Phys Chem C 111:7845–7847
31. Qian H, Eckenhoff WT, Bier ME, Pintauer T, Jin R (2011) Crystal structures of Au_2 complex and Au_{25} nanocluster and mechanistic insight into the conversion of polydisperse nanoparticles into monodisperse Au_{25} nanoclusters. Inorg Chem 50:10735–10739
32. Das A, Li T, Nobusada K, Zeng Q, Rosi NL, Jin R (2012) Total structure and optical properties of a phosphine/thiolate-protected Au_{24} nanocluster. J Am Chem Soc 134:20286–20289

33. Yang H, Wang Y, Lei J, Shi L, Wu X, Mäkinen V, Lin S, Tang Z, He J, Häkkinen H, Zheng L, Zheng N (2013) Ligand-stabilized $Au_{13}Cu_x$ (x = 2, 4, 8) bimetallic nanoclusters: ligand engineering to control the exposure of metal sites. J Am Chem Soc 135:9568–9571
34. Brust M, Walker M, Bethell D, Schiffrin DJ, Whyman R (1994) Synthesis of thiol-derivatized gold nanoparticles in a two-phase liquid-liquid system. J Chem Soc Chem Commun 7:801–802
35. Whetten RL, Khoury JT, Alvarez MM, Murthy S, Vezmar I, Wang ZL, Stephens PW, Cleveland CL, Luedtke WD, Landman U (1996) Nanocrystal Gold Molecules. Adv Mater 8: 428–433
36. Alvarez MM, Khoury JT, Schaaff TG, Shafigullin MN, Vezmar I, Whetten RL (1997) Optical absorption spectra of nanocrystal gold molecules. J Phys Chem B 101:3706–3712
37. Jin R, Qian H, Wu Z, Zhu Y, Zhu M, Mohanty A, Garg N (2010) Size focusing: a methodology for synthesizing atomically precise gold nanoclusters. J Phys Chem Lett 1:2903–2910
38. Zhu M, Lanni E, Garg N, Bier ME, Jin R (2008) Kinetically controlled, high-yield synthesis of Au_{25} clusters. J Am Chem Soc 130:1138–1139
39. Qian H, Zhu Y, Jin R (2009) Size-focusing synthesis, optical and electrochemical properties of monodisperse $Au_{38}(SC_2H_4Ph)_{24}$ nanoclusters. ACS Nano 3:3795–3803
40. Qian H, Jin R (2009) Controlling nanoparticles with atomic precision: the case of $Au_{144}(SCH_2CH_2Ph)_{60}$. Nano Lett 9:4083–4087
41. Qian H, Zhu Y, Jin R (2012) Atomically precise gold nanocrystal molecules with surface plasmon resonance. Proc Natl Acad Sci U S A 109:696–700
42. Shichibu Y, Negishi Y, Tsukuda T, Teranishi T (2005) Large-scale synthesis of thiolated Au_{25} clusters via ligand exchange reactions of phosphine-stabilized Au_{11} clusters. J Am Chem Soc 127:13464–13465
43. Nimmala PR, Dass A (2011) $Au_{36}(SPh)_{23}$ nanomolecules. J Am Chem Soc 133:9175–9177
44. Cleveland CL, Landman U, Schaaff TG, Shafigullin MN, Stephens PW, Whetten RL (1997) Structural evolution of smaller gold nanocrystals: the truncated decahedral motif. Phys Rev Lett 79:1873–1876
45. Schaaff TG, Shafigullin MN, Khoury JT, Vezmar I, Whetten RL, Cullen WG, First PN, Gutierrez-Wing C, Ascensio J, Jose-Yacaman MJ (1997) Isolation of smaller nanocrystal au molecules: robust quantum effects in optical spectra. J Phys Chem B 101:7885–7891
46. Schaaff TG, Knight G, Shafigullin MN, Borkman RF, Whetten RL (1998) Isolation and selected properties of a 10.4 kDa gold: glutathione cluster compound. J Phys Chem B 102: 10643–10646
47. Schaaff TG, Shafigullin MN, Khoury JT, Vezmar I, Whetten RL (2001) Properties of a ubiquitous 29 kDa Au: SR cluster compound. J Phys Chem B 105:8785–8796
48. Chaki NK, Negishi Y, Tsunoyama H, Shichibu Y, Tsukuda T (2008) Ubiquitous 8 and 29 kDa Gold:Alkanethiolate cluster compounds: mass-spectrometric determination of molecular formulas and structural implications. J Am Chem Soc 130:8608–8610
49. Tsunoyama H, Negishi Y, Tsukuda T (2006) Chromatographic isolation of "Missing" Au_{55} clusters protected by alkanethiolates. J Am Chem Soc 128:6036–6037
50. Qian H, Zhu Y, Jin R (2010) Isolation of ubiquitous $Au_{40}(SR)_{24}$ clusters from the 8 kDa gold clusters. J Am Chem Soc 132:4583–4585
51. Knoppe S, Boudon J, Dolamic I, Dass A, Burgi T (2011) Size exclusion chromatography for semipreparative scale separation of $Au_{38}(SR)_{24}$ and $Au_{40}(SR)_{24}$ and larger clusters. Anal Chem 83:5056–5061
52. Qian H, Jin R (2011) Synthesis and electrospray mass spectrometry determination of thiolate-protected $Au_{55}(SR)_{31}$ nanoclusters. Chem Comm 47:11462–11464
53. Negishi Y, Sakamoto C, Ohyama T, Tsukuda T (2012) Synthesis and the origin of the stability of thiolate-protected Au_{130} and Au_{187} clusters. J Phys Chem Lett 3:1624–1628
54. Nimmala PR, Yoon B, Whetten RL, Landman U, Dass A (2013) $Au_{67}(SR)_{35}$ nanomolecules: characteristic size-specific optical, electrochemical, structural properties and first-principles theoretical analysis. J Phys Chem A 117:504–517

55. Schaaff TG, Whetten RL (1999) Controlled etching of Au:SR cluster compounds. J Phys Chem B 103:9394–9396
56. Sakai N, Tatsuma T (2010) Photovoltaic properties of glutathione-protected gold clusters adsorbed on TiO_2 electrodes. Adv Mater 22:3185–3188
57. Sexton JZ, Ackerson CJ (2010) Determination of rigidity of protein bound Au_{144} clusters by electron cryomicroscopy. J Phys Chem C 114:16037–16042
58. Wu Z, Wang M, Yang J, Zheng X, Cai W, Meng G, Qian H, Wang H, Jin R (2012) Well-defined nanoclusters as fluorescent nanosensors: a case study on $Au_{25}(SG)_{18}$. Small 8:2028–2035
59. Li G, Jin R (2013) Atomically precise gold nanoclusters as new model catalysts. Acc Chem Res 46:1749–1758
60. Wu Z, MacDonald M, Chen J, Zhang P, Jin R (2011) Kinetic control and thermodynamic selection in the synthesis of atomically precise gold nanoclusters. J Am Chem Soc 133: 9670–9673
61. Akola J, Walter M, Whetten RL, Häkkinen H, Grönbeck H (2008) On the structure of thiolate-protected Au_{25}. J Am Chem Soc 130:3756–3757
62. Wu Z, Suhan J, Jin R (2009) One-pot synthesis of atomically monodisperse, thiol-functionalized Au_{25} nanoclusters. J Mater Chem 19:622–626
63. Liu C, Li G, Pang G, Jin R (2013) Toward understanding the growth mechanism of $Au_n(SR)_m$ nanoclusters: effect of solvent on cluster size. RSC Adv 3:9778–9784
64. Dharmaratne AC, Krick T, Dass A (2009) Nanocluster size evolution studied by mass spectrometry in room temperature $Au_{25}(SR)_{18}$ synthesis. J Am Chem Soc 131:13604–13605
65. Qian H, Liu C, Jin R (2012) Controlled growth of molecularly pure $Au_{25}(SR)_{18}$ and $Au_{38}(SR)_{24}$ nanoclusters from the same polydispersed crude product. Sci China Chem 55: 2359–2365
66. Stellwagen D, Weber A, Bovenkamp GL, Jin R, Bitter JH, Kumar CSSR (2012) Ligand control in thiol stabilized Au_{38} clusters. RSC Adv 2:2276–2283
67. Qian H, Jin R (2011) Ambient synthesis of $Au_{144}(SR)_{60}$ nanoclusters in methanol. Chem Mater 23:2209–2217
68. Zhu M, Qian H, Jin R (2009) Thiolate-protected Au_{20} clusters with a large energy gap of 2.1 eV. J Am Chem Soc 131:7220–7221
69. Zhu M, Qian H, Jin R (2010) Thiolate-protected $Au_{24}(SC_2H_4Ph)_{20}$ nanoclusters: superatoms or not? J Phys Chem Lett 1:1003–1007
70. Levi-Kalisman Y, Jadzinsky PD, Kalisman N, Tsunoyama H, Tsukuda T, Bushnell DA, Kornberg RD (2011) Synthesis and characterization of Au_{102}(p-MBA)$_{44}$ nanoparticles. J Am Chem Soc 133:2976–2983
71. Xu Q, Wang S, Liu Z, Xu G, Meng X, Zhu M (2013) Synthesis of selenolate-protected $Au_{18}(SeC_6H_5)_{14}$ nanoclusters. Nanoscale 5:1176–1182
72. Yu Y, Chen X, Yao Q, Yu Y, Yan N, Xie J (2013) Scalable and precise synthesis of thiolated $Au_{10–12}$, Au_{15}, Au_{18}, and Au_{25} nanoclusters via pH controlled CO reduction. Chem Mater 25: 946–952
73. Ghosh A, Udayabhaskararao T, Pradeep T (1997–2002) One-step route to luminescent $Au_{18}SG_{14}$ in the condensed phase and its closed shell molecular ions in the gas phase. J Phys Chem Lett 2012:3
74. Zeng C, Liu C, Pei Y, Jin R (2013) Thiol ligand-induced transformation of $Au_{38}(SC_2H_4Ph)_{24}$ to Au_{36}(SPh-*t*-Bu)$_{24}$. ACS Nano 7:6138–6145
75. Whetten RL, Price RC (2007) Nano-golden order. Science 318:407–408
76. Jiang D, Tiago ML, Luo W, Dai S (2008) The "Staple" Motif: a key to stability of thiolate-protected gold nanoclusters. J Am Chem Soc 130:2777–2779
77. Pei Y, Gao Y, Zeng XC (2008) Structural prediction of thiolate-protected Au_{38}: a face-fused bi-icosahedral Au core. J Am Chem Soc 130:7830–7832
78. Lopez-Acevedo O, Tsunoyama H, Tsukuda T, Häkkinen H, Aikens CM (2010) Chirality and electronic structure of the thiolate-protected Au_{38} nanocluster. J Am Chem Soc 132: 8210–8218

79. Jiang D-E, Overbury SH, Dai S (2013) Structure of $Au_{15}(SR)_{13}$ and its implication for the origin of the nucleus in thiolated gold nanoclusters. J Am Chem Soc 135:8786–8789
80. Pei Y, Gao Y, Shao N, Zeng XC (2009) Thiolate-protected $Au_{20}(SR)_{16}$ cluster: prolate Au_8 core with new $[Au_3(SR)_4]$ staple Motif. J Am Chem Soc 131:13619–13621
81. Iwasa T, Nobusada K (2007) Theoretical investigation of optimized structures of thiolated gold cluster $[Au_{25}(SCH_3)_{18}]^+$. J Phys Chem C 111:45–49
82. Jin R, Zhu Y, Qian H (2011) Quantum-sized gold nanoclusters: bridging the gap between organometallics and nanocrystals. Chem Eur J 17:6584–6593
83. Venzo A, Antonello S, Gascón JA, Guryanov I, Leapman RD, Perera NV, Sousa A, Zamuner M, Zanella A, Maran F (2011) Effect of the charge state (z = −1, 0, +1) on the nuclear magnetic resonance of monodisperse $Au_{25}[S(CH_2)_2Ph]_{18}^z$ clusters. Anal Chem 83: 6355–6362
84. Liu Z, Zhu M, Meng X, Xu G, Jin R (2011) Electron transfer between $[Au_{25}(SC_2H_4Ph)_{18}]^-TOA^+$ and oxoammonium cations. J Phys Chem Lett 2:2104–2109
85. Negishi Y, Chaki NK, Shichibu Y, Whetten RL, Tsukuda T (2007) Origin of magic stability of thiolated gold clusters: a case study on $Au_{25}(SC_6H_{13})_{18}$. J Am Chem Soc 129:11322–11323
86. Parker JF, Choi J-P, Wang W, Murray RW (2008) Electron self-exchange dynamics of the nanoparticle couple $[Au_{25}(SC_2Ph)_{18}]^{0/1-}$ by nuclear magnetic resonance line-broadening. J Phys Chem C 112:13976–13981
87. Kwak K, Lee D (2012) Electrochemical characterization of water-soluble Au_{25} nanoclusters enabled by phase-transfer reaction. J Phys Chem Lett 3:2476–2481
88. Swanick KN, Hesari M, Workentin MS, Ding Z (2012) Interrogating near-infrared electrogenerated chemiluminescence of $Au_{25}(SC_2H_4Ph)_{18}^+$ clusters. J Am Chem Soc 134: 15205–15208
89. Zhu M, Aikens CM, Hendrich MP, Gupta R, Qian H, Schatz GC, Jin R (2009) Reversible switching of magnetism in thiolate-protected Au_{25} superatoms. J Am Chem Soc 131: 2490–2492
90. Marks L (1983) Modified Wulff constructions for twinned particles. J Cryst Growth 61: 556–566
91. Marks L (1984) Surface structure and energetics of multiply twinned particles. Philos Mag A 49:81–93
92. Mednikov EG, Dahl LF (2008) Crystallographically proven nanometer-sized gold thiolate cluster $Au_{102}(SR)_{44}$: its unexpected molecular anatomy and resulting stereochemical and bonding consequences. Small 4:534–537